

## **Chapter 3. Low Temperature Preparation and Properties of Sol-Gel Derived Ti-rich $\text{Pb}(\text{Zr}_{1-x}\text{Ti}_x)\text{O}_3$ Thin Films**

This chapter is divided into two parts. In the first part, Ti-rich PZT films are intensively investigated for their structural and electrical properties as a function of Ti content. In the second part, the integration of Ti-rich PZT films into the currently used diffusion barrier is discussed.

### **3.1 INTRODUCTION**

The solid-solution PZT has a wide range of ferroelectric phase transition temperatures (Curie-temperatures) and two different ferroelectric structures, depending on the Zr/Ti composition ratio [1]. Figure 3.1 shows the phase diagram of PZT in which the phase transitions are observed. When the Ti content is higher than 0.47, PZT transforms from cubic structure to tetragonal structure at the temperatures ranging from 370 to 490 °C. When the Ti content is lower than 0.47, there is a cubic to rhombohedral transition with Curie-temperatures ranging from 230 to 370 °C. The phase diagram clearly shows that the Curie-temperatures of PZT increase as the Ti content increases. It is required for the ferroelectric memory to have a wide range of operating temperatures within which the electrical properties are maintained constant. There is morphotropic phase boundary (MPB) region in which the tetragonal and rhombohedral structures are coexisted. The mixture of these two structures in MPB region gives good ferroelectric properties to the PZT films at  $\text{Ti} = 0.47$ . The lattice parameters of tetragonal structure are changed as a function of Zr/Ti ratio. It was observed that  $c/a$  lattice ratio decreased as the Ti content increased [2]. Figure 3.2 shows the dependence of lattice parameters on the PZT composition. PZT thin films and bulk data were given for comparison. The a-axis and b-axis

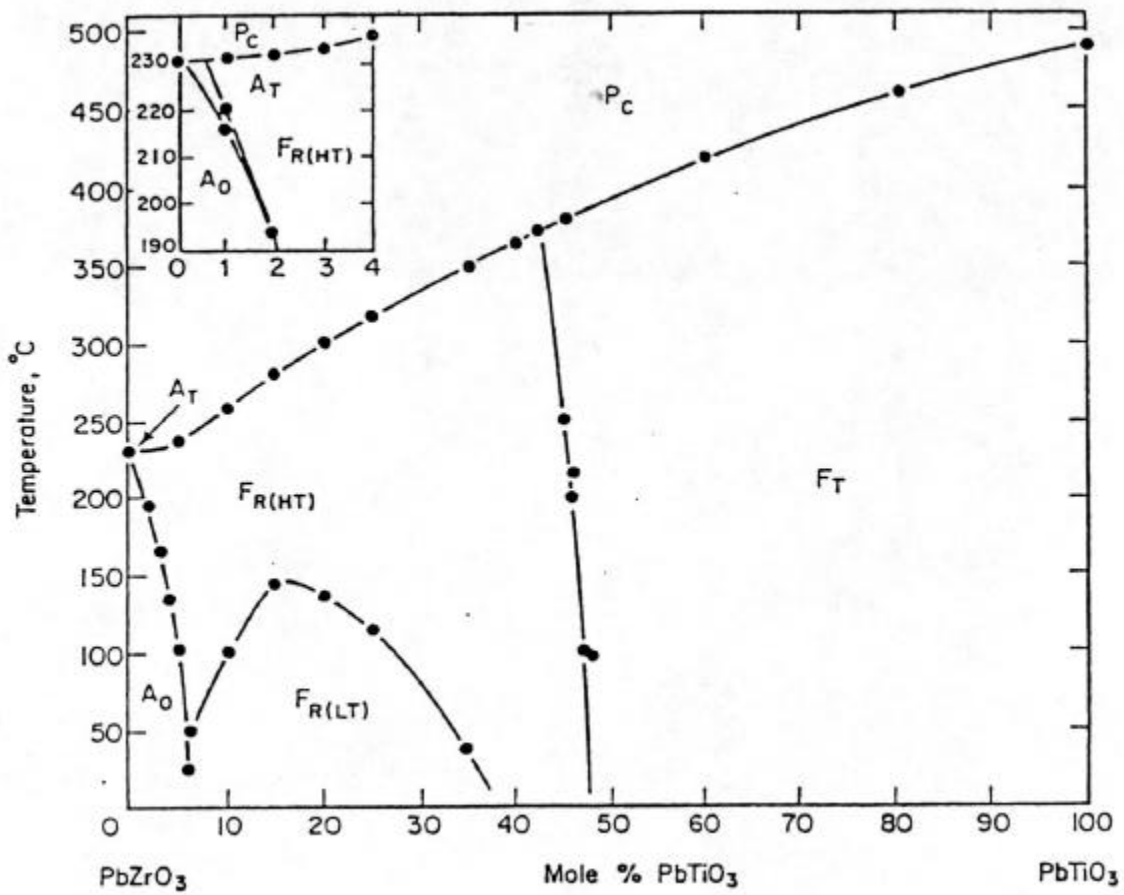


Figure 3.1 Phase diagram of lead zirconate titanate [1].

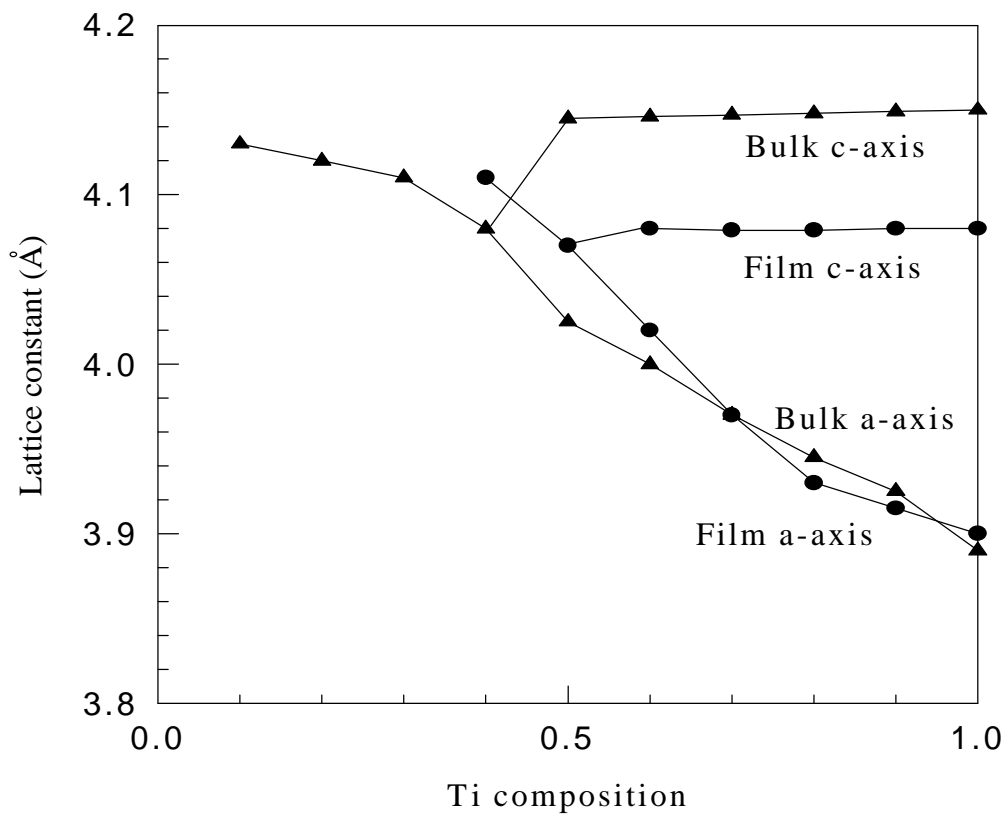


Figure 3.2 Lattice parameters of PZT bulk and thin films [2].

lattice parameters of PZT thin films almost correspond to those of the bulk ceramics, whereas the values of c-axis lattice parameter are slightly smaller than those of the bulk. This difference might be attributed to the orientation of the PZT thin films and/or the stress caused by the difference in thermal expansion coefficient between the films and Pt substrate rather than the deviation of composition. The Ti-rich PZT films show the tetragonal structure whose unit cell distortion (c/a ratio) increases as the Ti content increases.

The PZT oxide system is basically a solid solution of  $\text{PbTiO}_3$  (PT) and  $\text{PbZrO}_3$  (PZ). PZT with Zr/Ti ratios from around 92/8 all the way up to 0/100 shows ferroelectric phases. Principally, PZT with Zr/Ti ratio in this range can be used in ferroelectric applications. There have been numerous researches on PZT films with various Zr/Ti composition ratio [3-5]. But practically, since the ferroelectric properties strongly rely on the composition, it is desired to determine the optimal composition for particular application. In general, the PZT films with 53/47 ratio (MPB region) have been intensively investigated for memory application, because these films exhibit largest  $P_r$  and lowest  $E_c$ , which are very important properties for the FRAM application. The Ti-rich PZT films are also considered as very attractive for process integration due to their low crystallization temperature. However, there have not been many reports of attempts to lower the processing temperature of Ti-rich PZT films and investigate their structural and electrical properties. Therefore, the objectives of this chapter are to prepare the Ti-rich PZT films at a lower annealing temperature, investigate their structural and electrical properties at various annealing temperature, and furthermore integrate the Ti-rich PZT films into the barrier layers at the low annealing temperature. For convenience, various  $\text{Pb}(\text{Zr}_{1-x}\text{Ti}_x)\text{O}_3$  films ( $x = 0.47, 0.6, 0.7,$  and  $0.8$ ) are denoted in this paper as PZT53/47, 40/60, 30/70, and 20/80, respectively.

In order to investigate the integration and electrical properties of the PZT films in the high density DRO FRAM devices, we construct a test substrate which has the same configuration

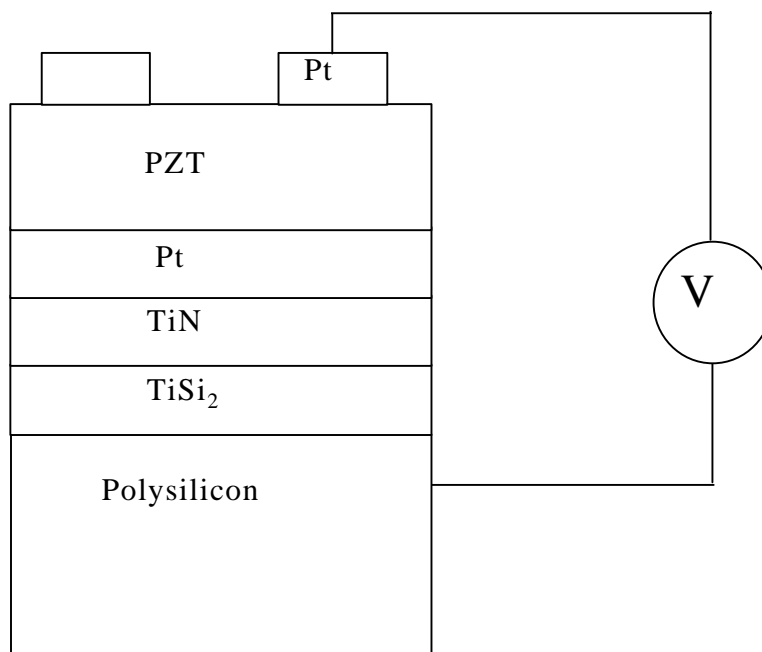


Figure 3.3 A test structure of ferroelectric capacitor in high density DRO FRAM devices.

as the ferroelectric capacitor, shown in Figure 3.3. The scheme of the test structure is outlined as Pt/barrier layers/polysilicon. In this research, titanium silicide ( $\text{TiSi}_2$ ) and titanium nitride ( $\text{TiN}$ ) are used as diffusion barrier layers, because they exhibit low resistivities at relatively high temperature ( $<550\text{ }^\circ\text{C}$ ). The barrier layers are deposited on poly-Si substrate using DC sputtering technique. The PZT films are then prepared on the test substrate by a modified sol-gel processing technique and processed at various annealing temperatures for investigating the thermal stability of the integrated PZT capacitors. The integration of the PZT films into the test structure is characterized by measuring electrical properties between bottom polysilicon and top Pt. Well-saturated P-E hysteresis loop will be observed if the diffusion barrier layers maintain their electrical conductivity after heat-treatment at the ferroelectric processing temperature.

### 3.2 EXPERIMENTAL PROCEDURES

0.4 M Ti-rich  $\text{Pb}(\text{Zr}_{1-x}\text{Ti}_x)\text{O}_3$  solutions ( $x = 0.6 - 0.8$ ) were prepared by using modified sol-gel processing, which was developed in the previous chapter. The precursors used to synthesize the solutions were Zr-n-propoxide, Ti-isopropoxide, and lead-acetate. With using n-propanol as solvent, the optimal amount of acetic acid was added to the solutions for modifying the solutions on a molecular level, which resulted in homogeneous solutions. The exact weights of these precursors are described in detail in Appendix A. Once the Ti-rich PZT solution were prepared, the precursor solutions were deposited on Pt/Ti/SiO<sub>2</sub>/Si substrates using spin-coating technique. The as-deposited layer was baked on a hot plate in air at  $150\text{ }^\circ\text{C}$  to evaporate water, alcohol and the organics. The spin-coating and drying process was repeated three times, and then the PZT films were finally annealed at various temperatures ranging from  $450$  to  $650\text{ }^\circ\text{C}$ . The PZT films were heat-treated in a pre-heated furnace under an oxygen atmosphere. After the heat-treatment,

the samples were taken out and cooled under room temperature condition. The final thickness of the PZT film with three layers was measured as about 0.25  $\mu\text{m}$  by ellipsometry.

The phase development of the films was investigated by X-ray diffraction (XRD) patterns, which were recorded on a Scintag XDS 2000 diffractometer using  $\text{CuK}\alpha$  radiation at 40 kV. The dielectric measurements were carried out at room temperature by using an HP 4192A impedance analyzer with a four-terminal extension configuration. For electrical measurements, Pt electrodes were deposited on the top surface of the films through a shadow mask by rf sputtering. The area of circular dots was measured as 0.00052  $\text{cm}^2$ . The ferroelectric properties were measured at room temperature using a standardized RT66A ferroelectric test system operating in a Virtual-Ground mode. The fatigue tests were performed under accelerated conditions using an externally generated square pulse with an amplitude of  $\pm 5$  V and a frequency of 1 MHz.

In order to integrate the PZT films into poly-Si substrates, the currently used barrier layers were prepared on poly-Si substrates by depositing the following structure: TiN (150 nm)/TiSi<sub>2</sub> (100 nm)/poly-Si. The poly-Si substrates were precleaned using a dilute HF solution to eliminate native SiO<sub>2</sub> oxide layer. Ti metal layer was then deposited at room temperature on clean poly-Si substrate in Ar atmosphere by DC sputtering. The Ar gas pressure and deposition rate was  $7 \times 10^{-3}$  torr and 50 nm/min, respectively. The Ti metal deposited on poly-Si was heat-treated at 800 °C in vacuum to form titanium silicide. The silicide formation is followed by TiN sputter-deposition in a reactive atmosphere of N<sub>2</sub> and Ar mixture gas at 300 °C on the TiSi<sub>2</sub>/polysilicon substrate. Finally, Pt bottom electrode was sputter-deposited on TiN<sub>x</sub>/TiSi<sub>2</sub>/poly-Si substrate in Ar atmosphere. The Ar gas pressure and deposition rate were  $2 \times 10^{-3}$  and 50 nm, respectively. The final substrates were heat-treated at 500 °C for relieving the stress developed during the electrode-barrier substrate preparation. Without this thermal relieving, the PZT films on the substrates were peeled off due to the stress. The PZT films were prepared on the electrode-barrier substrates by a modified sol-gel processing.

### 3.3 STRUCTURAL AND ELECTRICAL PROPERTIES OF TI-RICH PZT FILMS

Figure 3.4 a), b), and c) show the XRD patterns of PZT films with various compositions (40/60, 30/70, and 20/80) as a function of annealing temperature. Using the modified sol-gel processing technique, it was possible to prepare highly oriented Ti-rich PZT films on Pt/Ti/SiO<sub>2</sub>/Si substrates at an annealing temperature of 500 °C, which is lower than that of PZT53/47 films (550 °C). As the annealing temperature increased, the perovskite peaks were enhanced due to further crystallization and grain growth. Figure 3.5 summarizes the XRD patterns of Ti-rich PZT films processed at 500 °C. It was found that the perovskite phase formation temperature decreased as the Ti content was increased. As observed in the highly (111) oriented PZT53/47 films, the Ti-rich PZT films displayed strong (111) orientation. Additionally, these films showed significant (100) orientation especially when the Ti content increased from 0.7 to 0.8. It has been observed that another type of preferred orientation can occur for a flat-face growth in certain direction with a minimum surface energy [6-7]. In the PZT films, the calculations, based on the dissociation energies for PbO, TiO<sub>2</sub>, and ZrO<sub>2</sub> as reference data for bonding energies, determined the lowest surface energy to be for the (100) plane [8]. Therefore, (100) orientation is preferred when the heterogeneous nucleation sites for specific direction are not available. In the PZT53/47 films, since the lattice parameters of (111) PZT are closely matched with those of Pt<sub>3</sub>Ti, strong (111) orientation was entirely dominant over (100) orientation. However, as the lattice parameters (*c/a* ratio) of PZT films were increased due to the change of Zr/Ti composition ratio, the lattice matching of (111) PZT with Pt<sub>3</sub>Ti was reduced, which gives more chance for (100) grains to grow. Therefore, the PZT20/80 films showed the appreciable (100) orientation as well as the (111) grain orientation. The effect of PZT composition on the phase development is to reduce the crystallization temperature and enhance

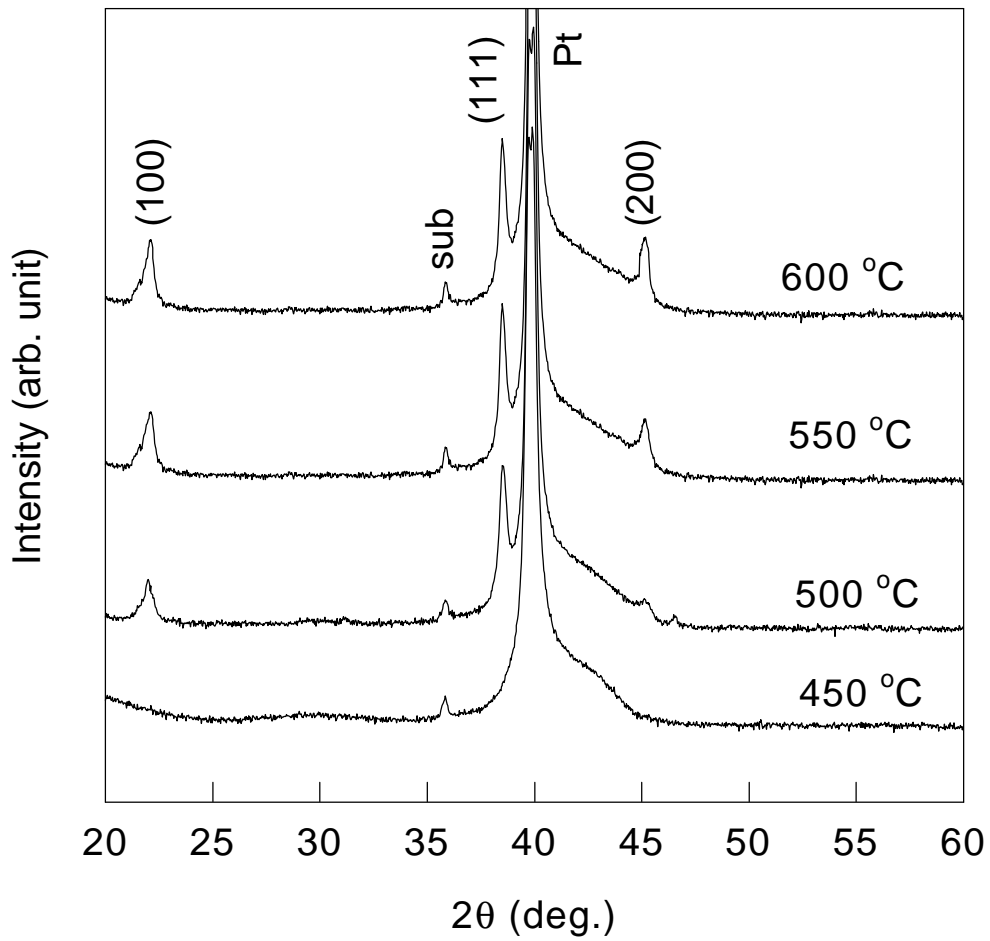


Figure 3.4 a) XRD patterns of PZT40/60 films as a function of annealing temperature.

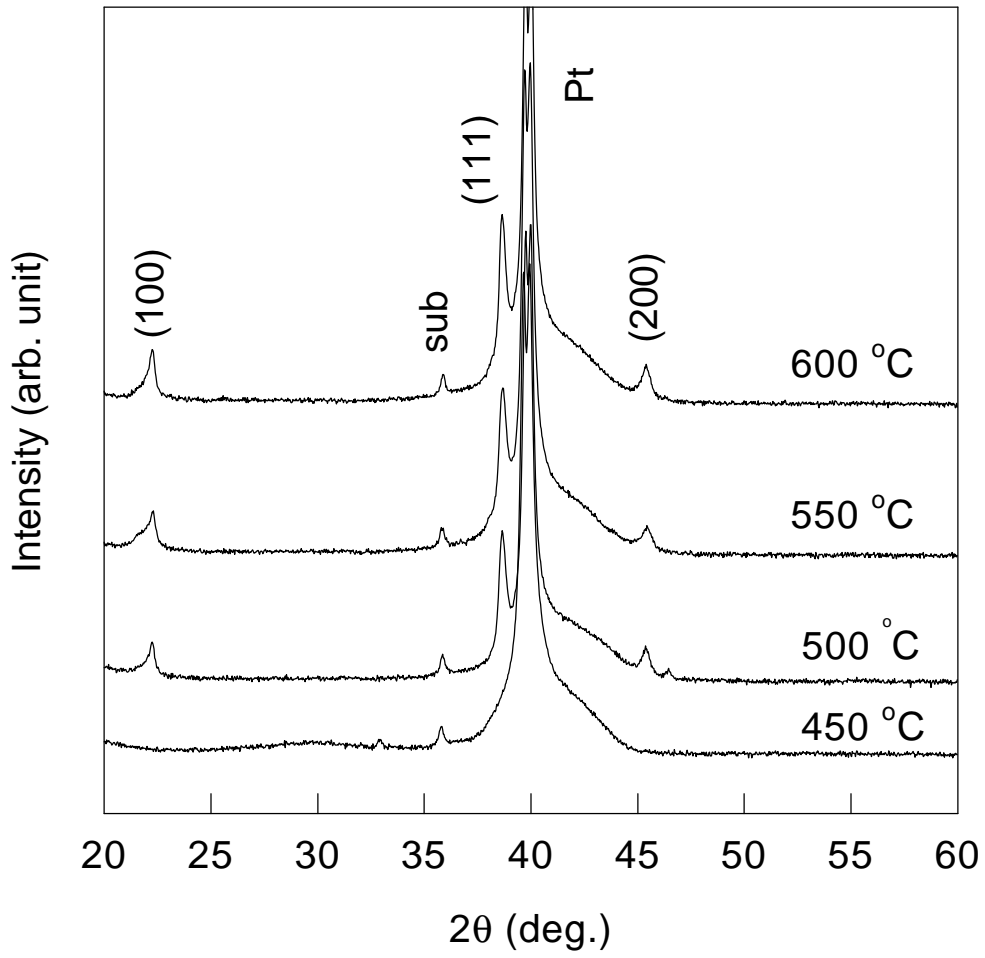


Figure 3.4 b) XRD patterns of PZT30/70 films as a function of annealing temperature.

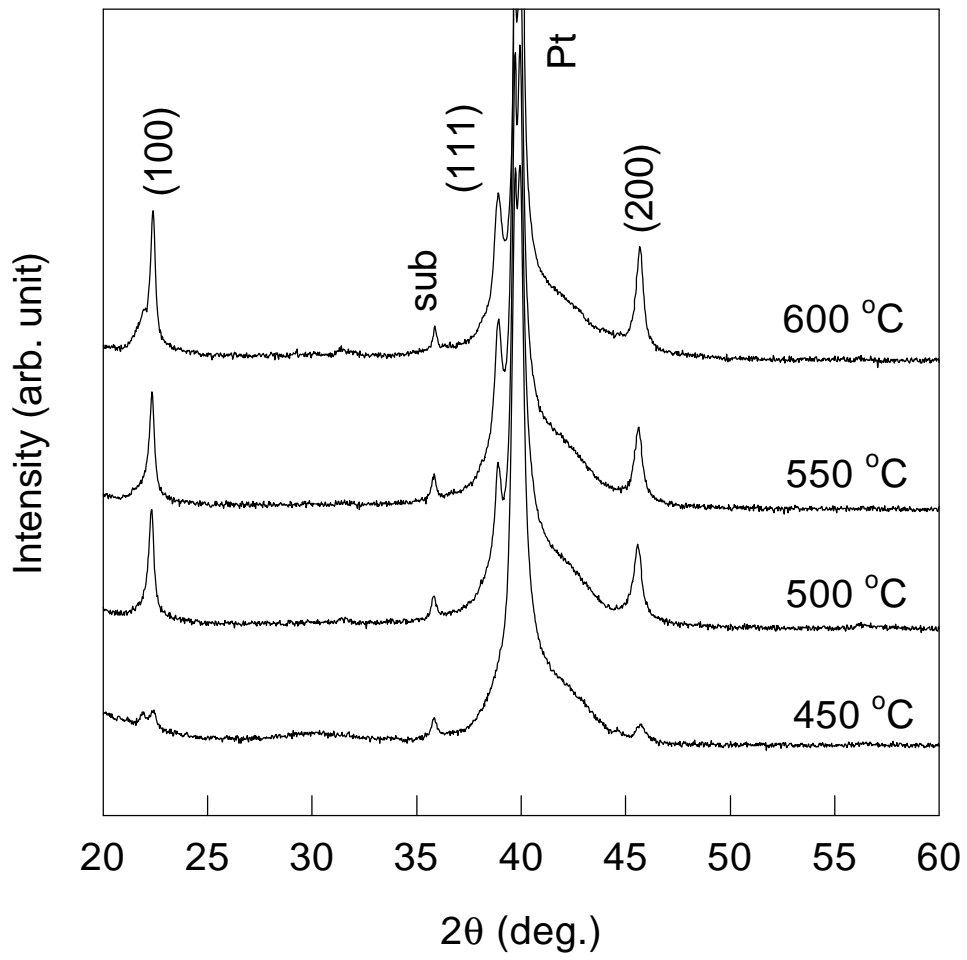


Figure 3.4 c) XRD patterns of PZT20/80 films as a function of annealing temperature.

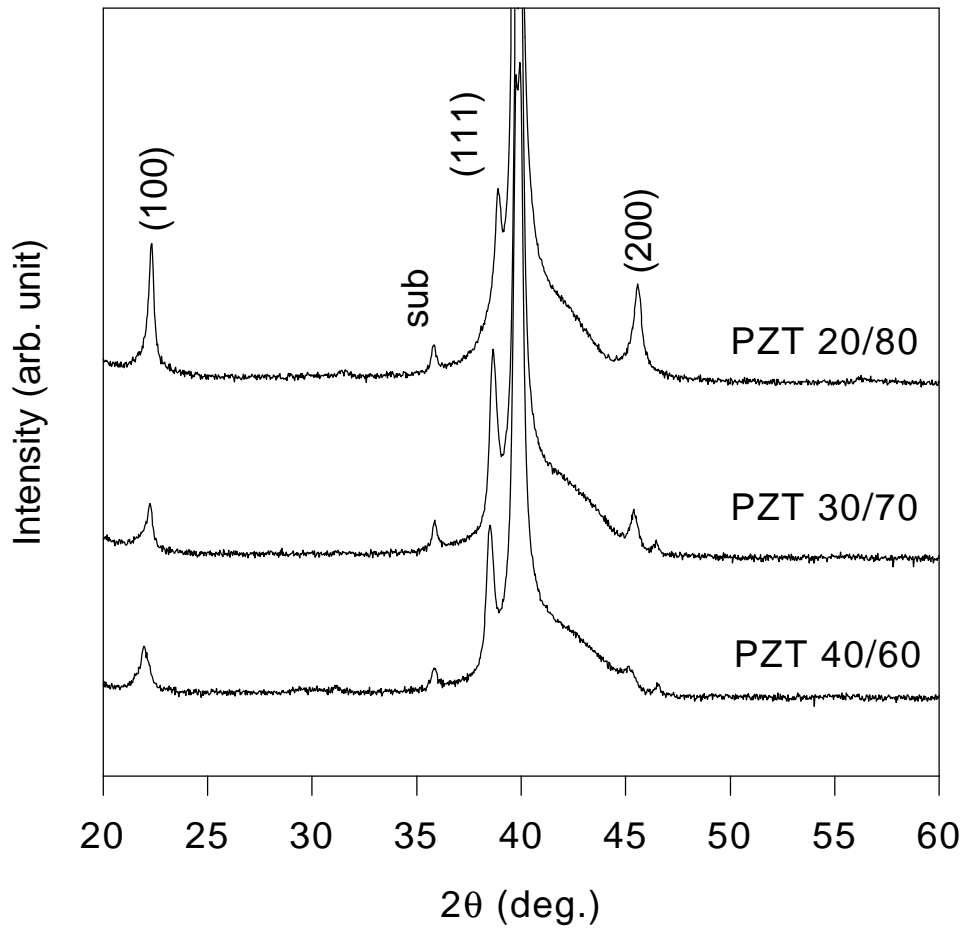


Figure 3.5 XRD patterns of PZT40/60, 30/70, and 20/80 films as an annealing temperature of 500 °C

(100) orientation as the Ti content increased.

Figure 3.6 a), b) and c) show the P-E hysteresis loops of Ti-rich PZT films annealed at 500 °C. Well-defined hysteresis loops were observed for the PZT films at a low annealing temperature of 500 °C. The  $P_r$  values were 5, 12, 14  $\mu\text{C}/\text{cm}^2$  for the PZT40/60, 30/70, and 20/80, respectively. The largest  $E_c$  was observed for the PZT20/80 films. It was found that the  $P_r$  increased as the Ti content increased. At an annealing temperature of 500 °C, the PZT20/80 films exhibited better enhancement in crystallization of perovskite phase than PZT40/60 and 30/70 films, because the perovskite phase formation temperature decreased as the Ti content increased. Therefore, the PZT20/80 films have better crystalline perovskite phase, and thus exhibited the largest  $P_r$  at 500 °C.

The ferroelectric properties of Ti-rich PZT films were investigated as a function of annealing temperature and Zr/Ti ratio. Figure 3.7 shows the dependence of  $P_r$  on the annealing temperature. For comparison,  $P_r$  and  $E_c$  values of PZT53/47 films were included. It has been reported that  $P_r$  is the highest for the PZT53/47 bulk and decreases as Ti content increases [1]. The reason for the largest  $P_r$  of PZT53/47 is that most domain switching orientations are possible at the morphotropic phase boundary (MPB) region. However, at the low annealing temperature of 500 °C, largest  $P_r$  was observed for the PZT20/80 films, which showed lower crystallization temperature than the PZT53/47, 40/60 and 30/70 films. The PZT20/80 films were almost completely crystallized into perovskite phase due to the low phase formation temperature. On the other hand, the perovskite phase of PZT53/47 films was not sufficiently developed at 500 °C to exhibit well-defined P-E hysteresis loops. As the annealing temperature increased from 500 to 550 °C, the  $P_r$  values of PZT53/47, 40/60, and 30/70 films considerably increased possibly due to the appreciable enhancement in crystallization of perovskite phase. In particular, a significant increase in the  $P_r$  value was observed for the PZT30/70 films, which showed the largest  $P_r$

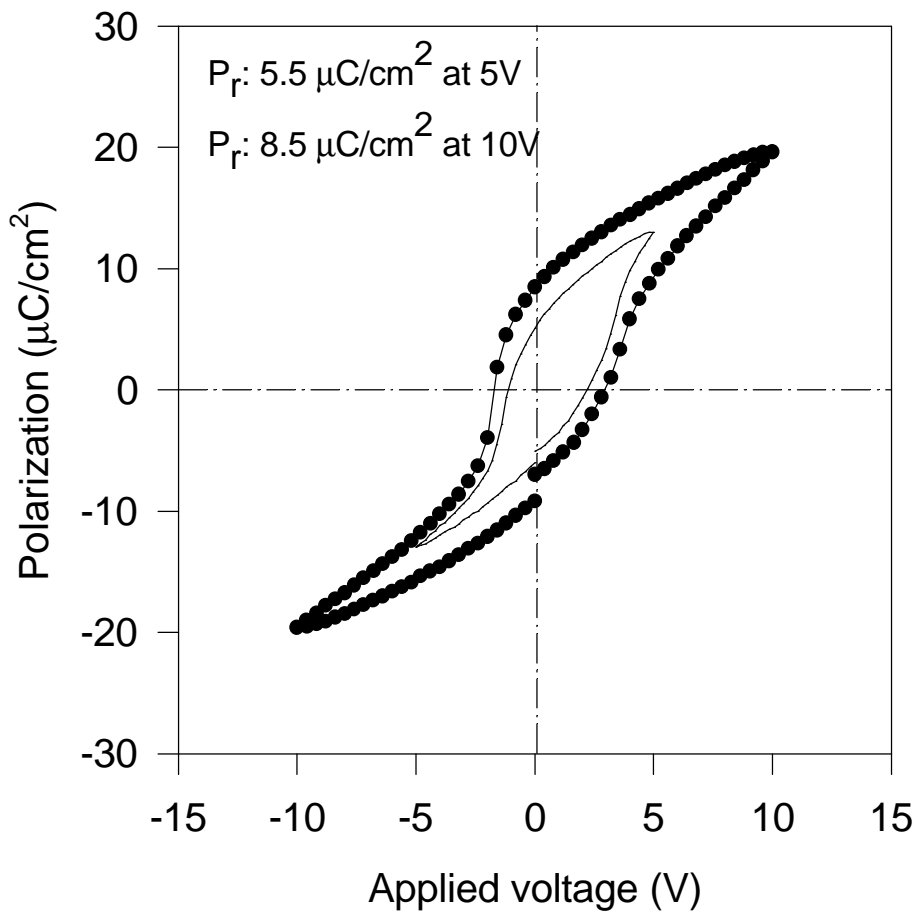


Figure 3.6 a) Hysteresis loop of PZT40/60 annealed at 500 °C.

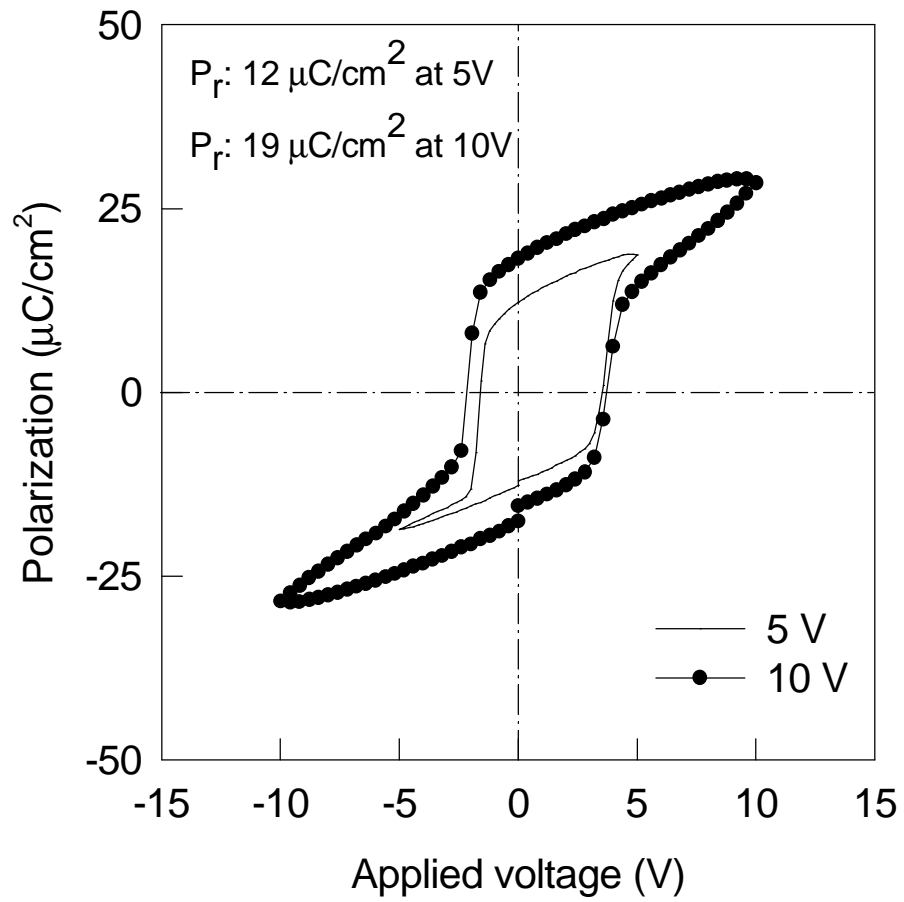


Figure 3.6 b) Hysteresis loop of PZT30/70 annealed at 500 °C.

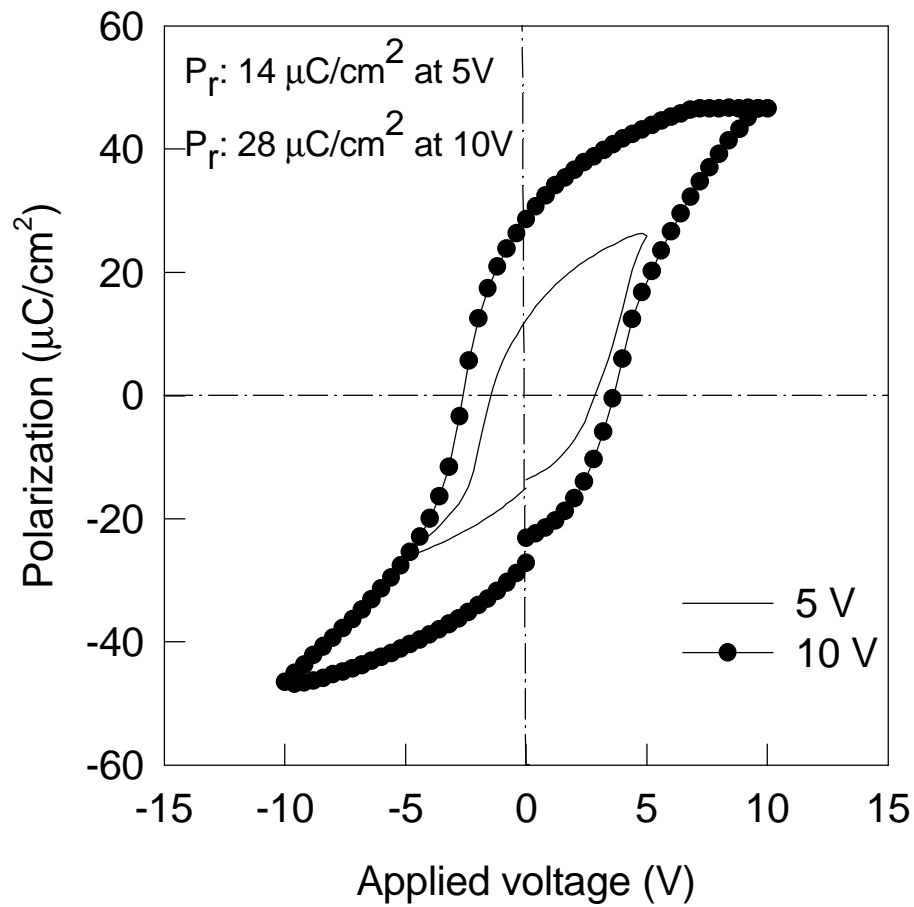


Figure 3.6 c) Hysteresis loop of PZT20/80 annealed at 500 °C.

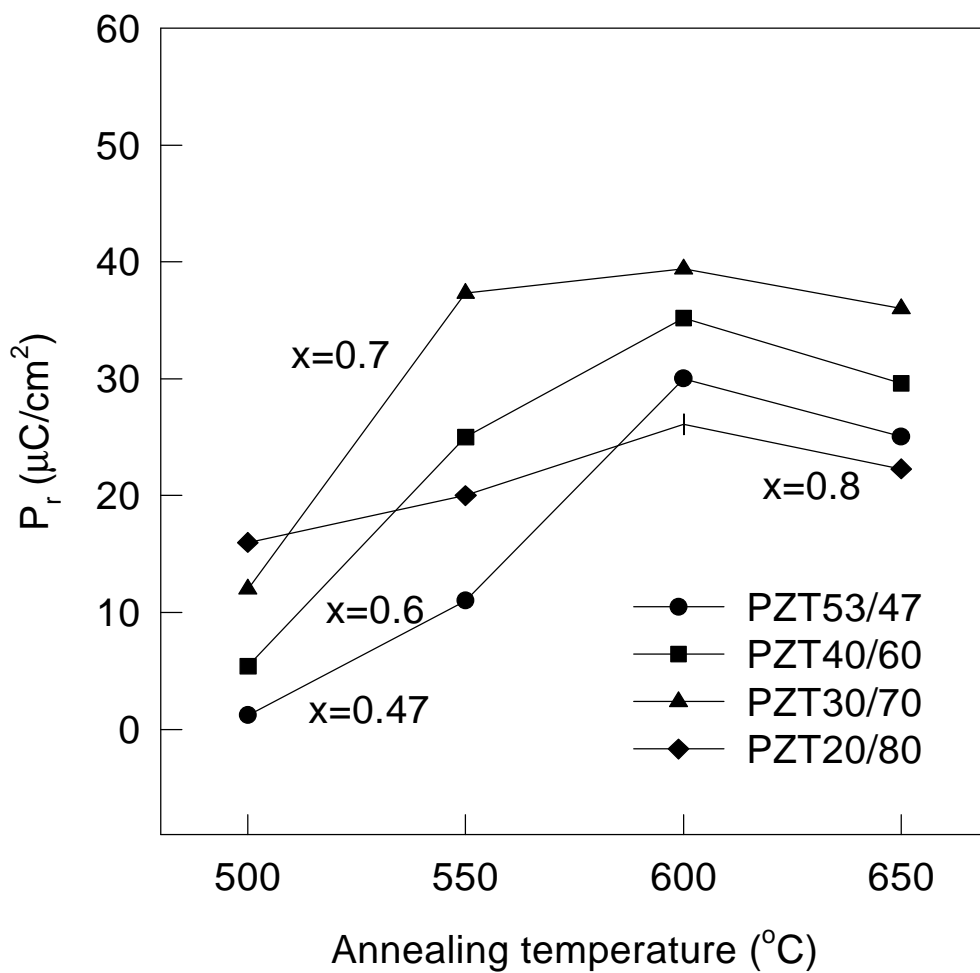


Figure 3.7 The dependence of  $P_r$  on the annealing temperature.

compared to PZT53/47, 40/60, and 20/80 films. On the other hand, the PZT20/80 films exhibited relatively smaller increase of  $P_r$  value. At 600 °C, only slight increase of  $P_r$  values was observed for PZT30/70 and 20/80 films, while the PZT53/47 and 40/60 films showed noticeable improvement of  $P_r$  value. At 650 °C, a little decrease of the  $P_r$  values was observed for the PZT films possibly due to lead loss at such a high annealing temperature.

Figure 3.8 shows the variation of  $P_r$  as a function of Zr/Ti ratio. The dependence of  $P_r$  value on the annealing temperature indicates the extent of perovskite phase crystallization at the specific annealing temperature. The larger  $P_r$  value of Ti-rich PZT films at the low temperature region means that the Ti-rich PZT films were relatively more crystallized into perovskite phase than PZT53/47 films at the low annealing temperature region. It was observed that the  $P_r$  value of PZT20/80 films showed little dependence on the annealing temperatures, implying the perovskite phase of PZT20/80 films was already fully crystallized at 500 °C. While the  $P_r$  values of PZT30/70 and 40/60 films substantially increased particularly as the annealing temperature increased from 500 to 550 °C, the PZT53/47 films showed a major increase of  $P_r$  value at the temperature ranging from 550 to 600 °C. The annealing temperature at which a significant increase of  $P_r$  value was observed, decreased as the Ti content increased. This could be attributed to the decrease of crystallization temperature with increase in Ti content. The  $P_r$  value showed a peak for the PZT30/70 at the annealing temperatures ranging from 550 to 650 °C. This trend is quite in contrast with the bulk data, but similar behavior was observed in other reports where the largest  $P_r$  value was observed for PZT20/80 films [9-10]. The maximum  $P_r$  for PZT30/70 films might be attributed to the strong (111) orientation observed for the PZT films.

Figure 3.9 shows the dependence of coercive field ( $E_c$ ) on the Zr/Ti composition ratio. The Ti content has a strong influence on the  $E_c$ . As the Ti content increased from 0.47 to 0.7, the  $E_c$  value significantly increased, but when the Ti content varied from 0.7 to 0.8, the  $E_c$  was

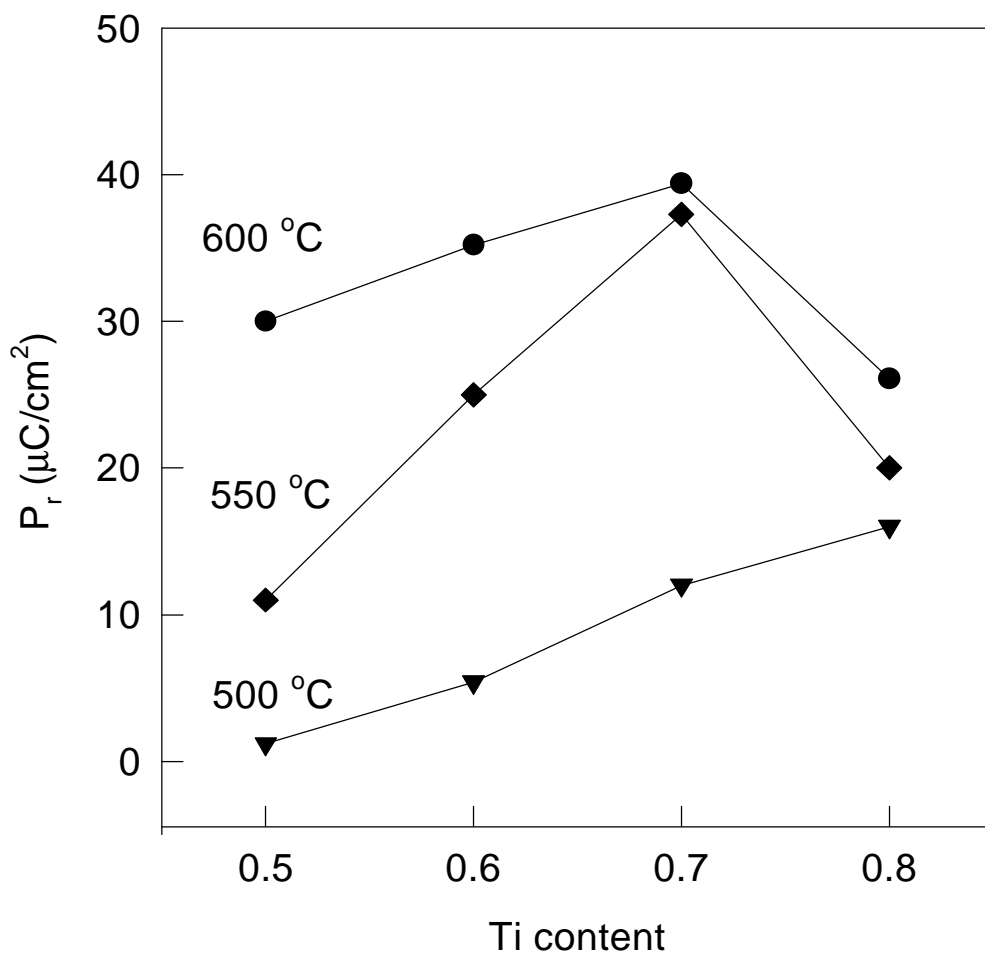


Figure 3.8 The variation of  $P_r$  as a function of Zr/Ti ratio.

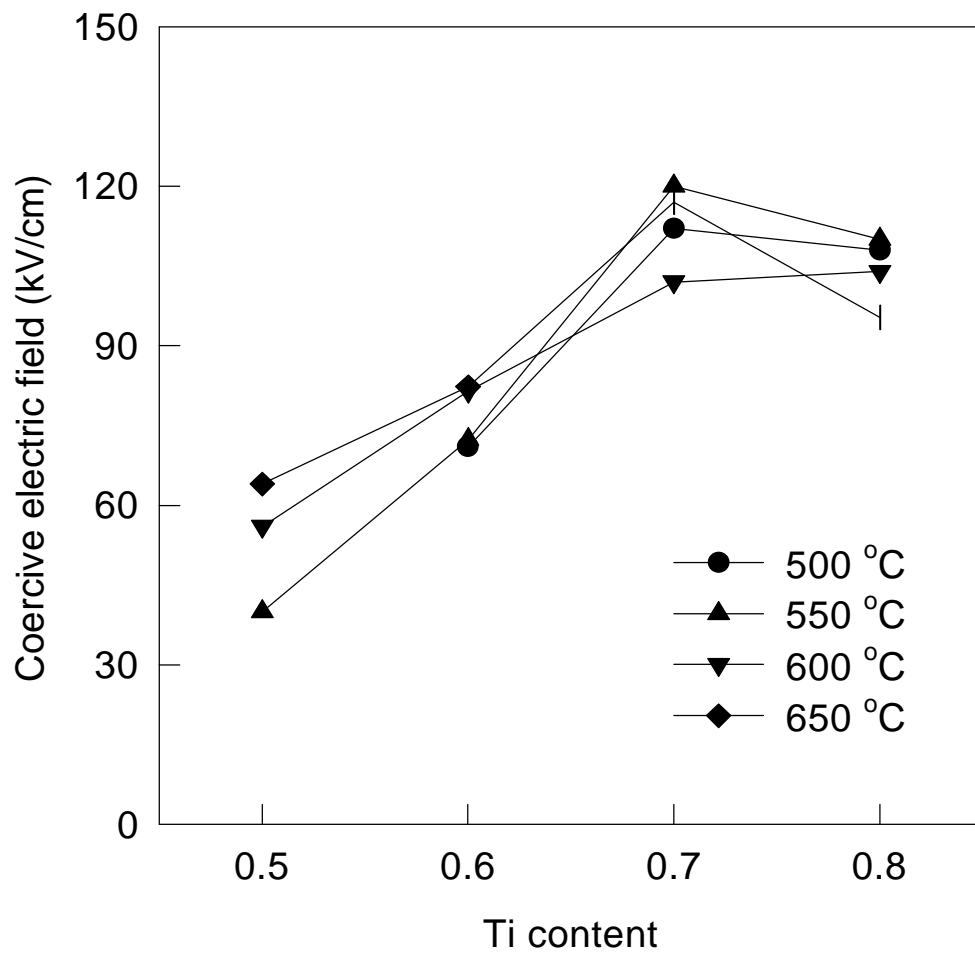


Figure 3.9 The variation of  $E_c$  as a function of Zr/Ti ratio.

almost the same or only slightly decreased. It was observed that this trend was almost independent of annealing temperature. On the whole,  $E_c$  was found to increase with increase in Ti content, irrespective of the annealing temperature.

Figure 3.10 shows the composition dependence of the small signal dielectric constant ( $\epsilon_r$ ) at 100 kHz for the PZT films at various annealing temperatures. At an annealing temperature of 500 °C, the  $\epsilon_r$  value increased as a function of Ti content. As the annealing temperature increased from 500 to 600 °C, the PZT53/47 showed a maximum  $\epsilon_r$  value of 1004, which was larger than the PZT bulk data [1], but similar to that of PZT films reported in other publications [11-12].<sup>19,20</sup> Typically, highly (111) oriented PZT films exhibited larger  $\epsilon_r$  than randomly oriented bulk ceramics. In addition, the tendency of  $\epsilon_r$  decreasing as a function of Ti content was in quite good agreement with the bulk data [1]. Figure 3.11 shows the variation of  $\epsilon_r$  as a function of annealing temperature for the PZT films. The  $\epsilon_r$  of PZT20/80 films was almost independent of the annealing temperature, while a major increase of  $\epsilon_r$  was observed for PZT40/60 and 30/70 films at the temperature region from 500 to 550 °C, and for PZT53/47 films at the temperatures ranging from 550 to 600 °C. This tendency was almost identical with that observed in the variation of  $P_r$ , and could be attributed to the decrease of perovskite phase formation temperature with the increase of Ti content, as mentioned earlier in the variation of  $P_r$ .

The fatigue properties of PZT30/70 films prepared on Pt/Ti/SiO<sub>2</sub>/Si substrates were investigated as a function of annealing temperature. The fatigue measurements were carried out at room temperature using a 1 MHz bipolar square pulse at an applied voltage of 5 V. The reason for selecting PZT30/70 films was that the films exhibited the largest  $P_r$  at the annealing temperatures ranging from 550 to 600 °C. Figure 3.12 illustrates fatigue test profiles of PZT30/70 films as a function of annealing temperature. The PZT30/70 films annealed at 600 °C showed lower degradation rate of polarization than at 500 °C and 550 °C. These results suggest

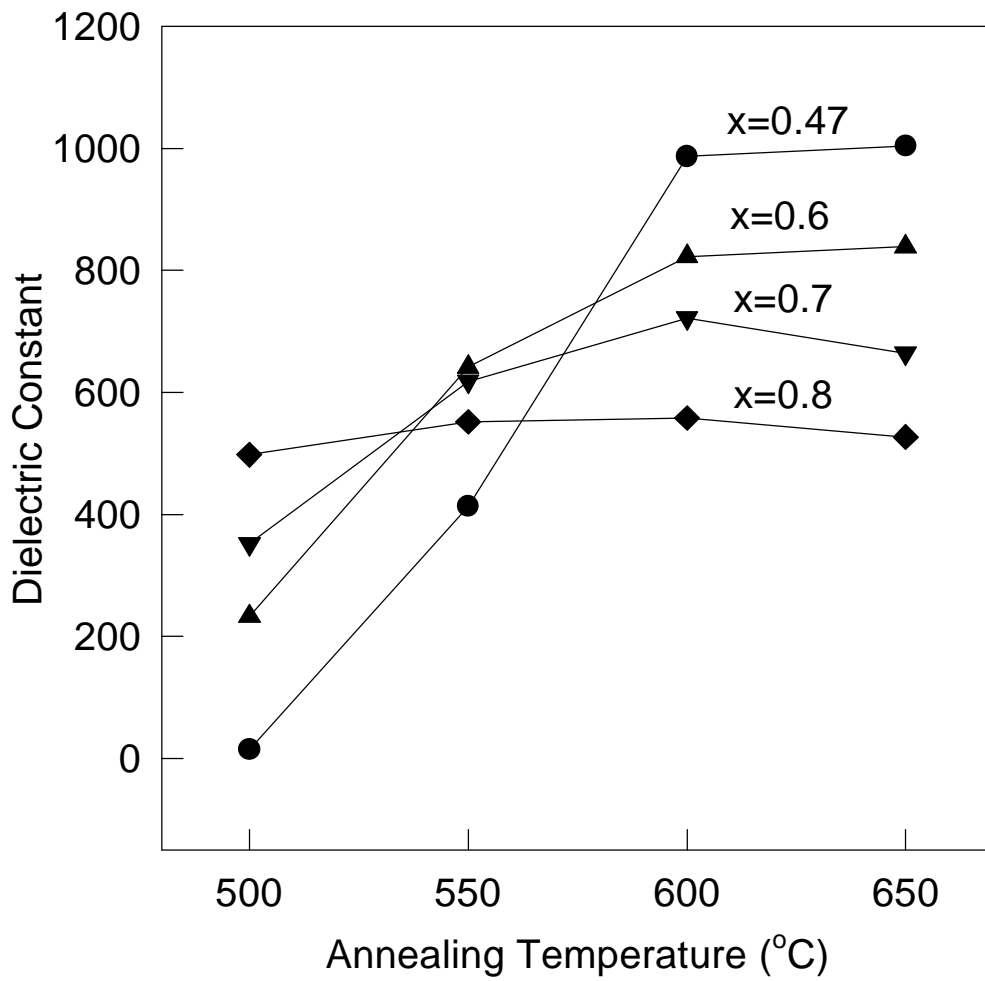


Figure 3.10 The composition dependence of  $\epsilon_r$  for PZT films at various annealing temperatures.

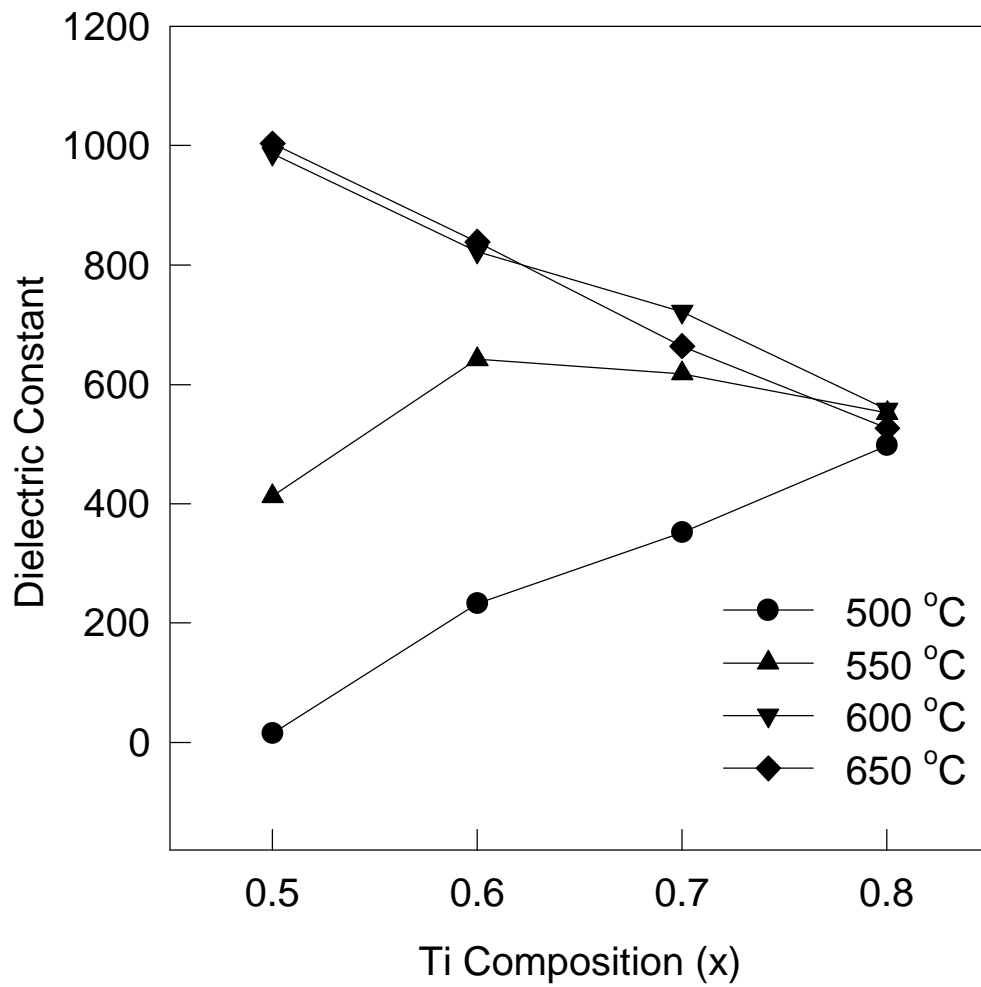


Figure 3.11 The variation of  $\epsilon_r$  for PZT films as a function of Zr/Ti ratio.

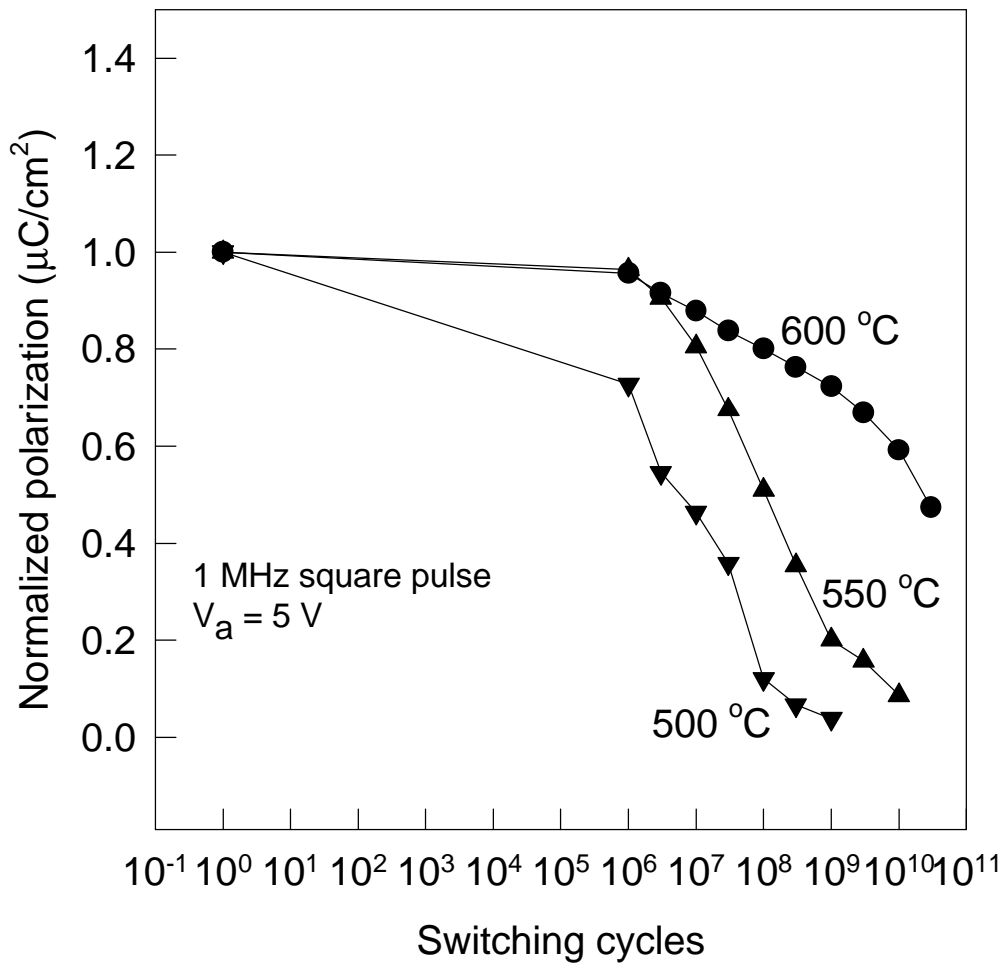


Figure 3.12 Fatigue test profiles of PZT30/70 films as a function of processing temperature.

that the enhancement in crystallization of perovskite phase may impede formation of second phase or any defect, which could work as domain pinning centers. The effect of Zr/Ti ratio on fatigue properties is illustrated on Figure 3.13. In order to obtain an appreciable remanent polarization value for PZT53/47 films, the PZT films with various compositions were annealed at high temperature of 600 °C. The PZT53/47 films showed worse fatigue properties than the PZT30/70 and 20/80 films, as observed in other reports [12]. It is interesting to note that the PZT30/70 and 20/80 films exhibited relatively better resistance to the polarization degradation than the PZT53/47 and 40/60 films. This results might be attributed to the better crystallization of perovskite phase in the PZT20/80 and 30/70 films, which showed the lower crystallization temperature than PZT53/47 and 40/60. The enhancement in crystallization reduces any possible second phases and defects, which act as domain pinning centers for the polarization degradation.

Current-voltage relationships were investigated at room temperature for the PZT films with various compositions annealed at 500 °C. Figure 3.14 shows the leakage current density of the PZT films as a function of applied voltage. Characteristic ferroelectric I-V curves were observed for the films, which exhibited good insulating properties even up to an applied voltage of 8 V. The leakage current density of the PZT40/60 films was  $10^{-7}$  A/cm<sup>2</sup> at an applied voltage of 10 V. As the Ti content increased, the PZT films showed high leakage current density at the same applied voltage, which might be attributed to the decrease in the density of the films with increase in Ti content.

### 3.4. INTEGRATION

The PZT30/70 films were prepared on Pt/TiN<sub>x</sub>/TiSi<sub>2</sub>/poly-Si substrate without any void or crack using the modified sol-gel processing. Figure 15 a) and b) show hysteresis loops of

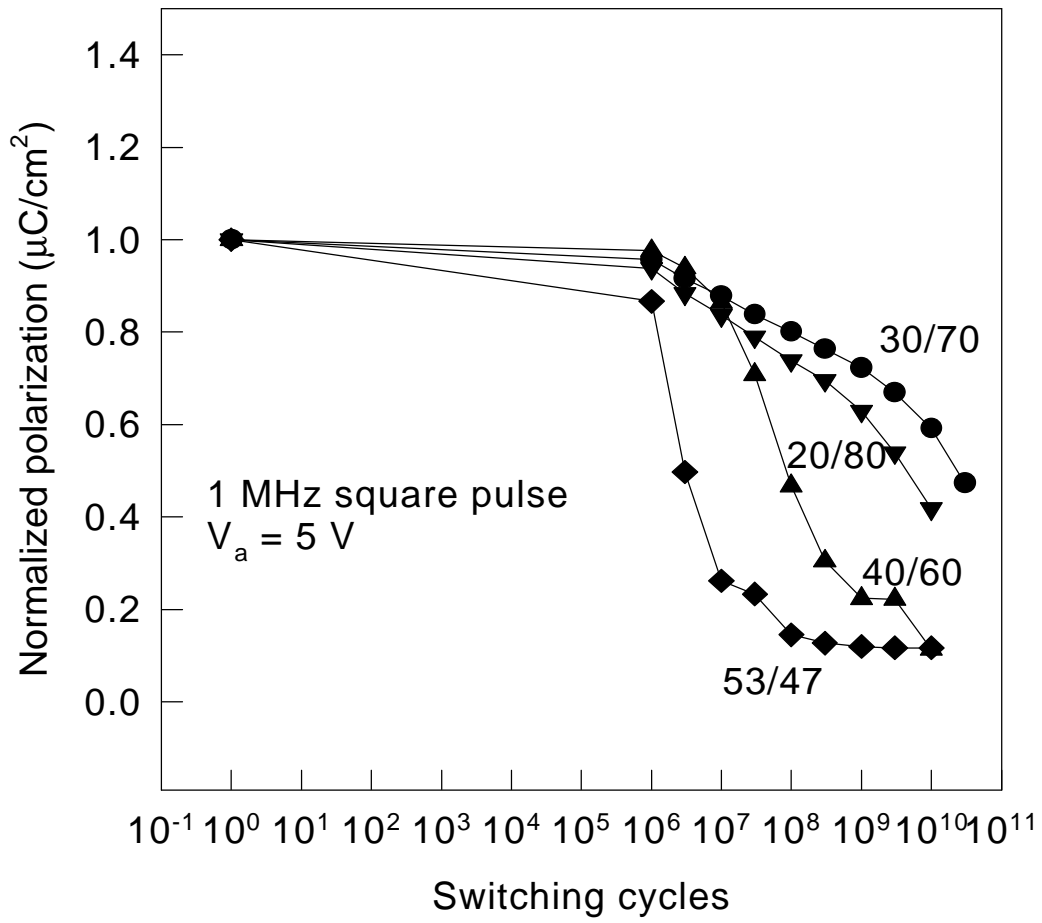


Figure 3.13 Fatigue test profiles of various PZT films annealed at 600 °C.

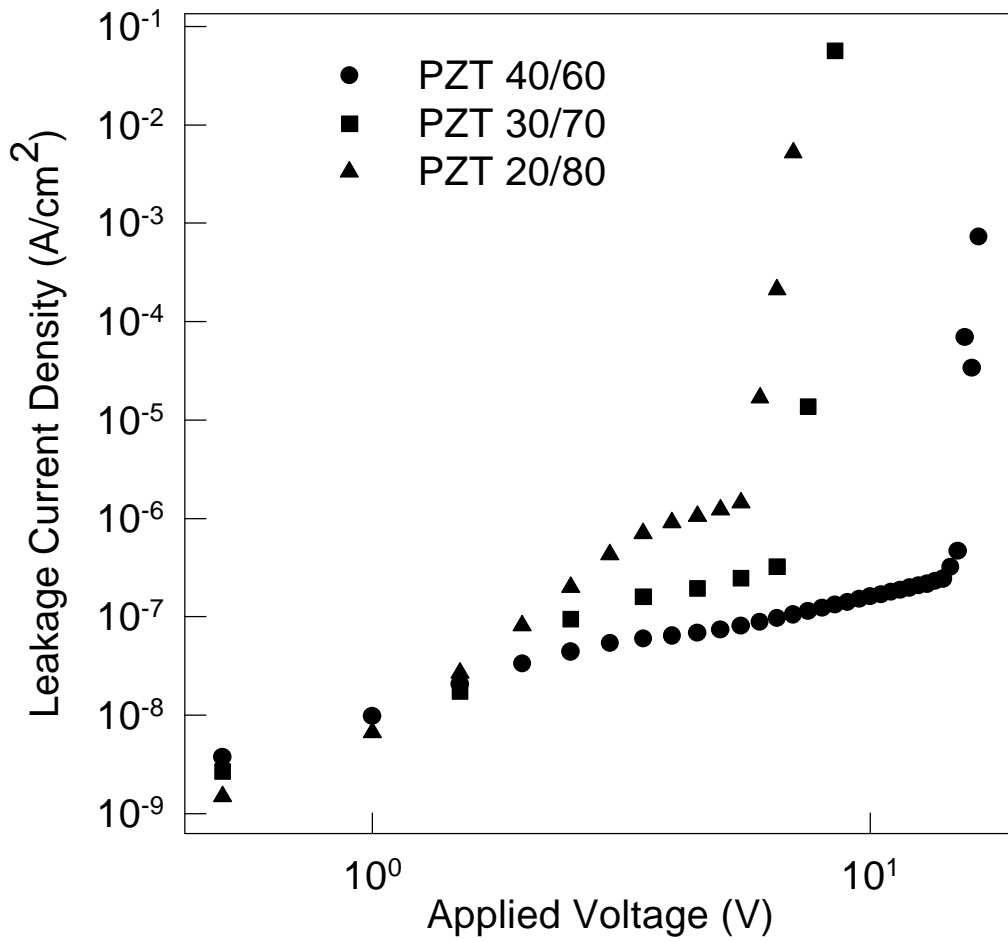


Figure 3.14 Leakage current density of various PZT films as a function of applied voltage.

PZT30/70 films annealed at 500 °C on Pt/TiN<sub>x</sub>/TiSi<sub>2</sub>/poly-Si substrate. Two hysteresis loops were observed by contacting between top Pt and bottom Pt or between top Pt and bottom poly-Si in order to investigate the thermal stability of the diffusion barrier layers after heat-treatment at 500 °C. Almost identical well-saturated P-E hysteresis loops were observed for the PZT30/70 films annealed at 500 °C, indicating that the barrier layers, TiN and TiSi<sub>2</sub>, do not form any undesired insulating layer, and are thermally stable at that processing temperature. However, as the annealing temperature increased from 500 to 550 and 600 °C, poor ferroelectric properties were observed for the PZT films on Pt/TiN<sub>x</sub>/TiSi<sub>2</sub>/poly-Si substrate, which means the barrier layers reacted with oxygen or ferroelectric films or poly-Si, and formed an insulating layer.

### 3.5. SUMMARY

1. Highly oriented Ti-rich PZT films ( $x = 0.60 - 0.80$ ) were successfully prepared on Pt/Ti/SiO<sub>2</sub>/Si substrates at a low annealing temperature of 500 °C by a modified sol-gel processing. As the Ti content increased, (100) orientation was enhanced due to the variation of lattice parameters.
2. Ferroelectric properties of PZT films were investigated as a function of Zr/Ti ratio and annealing temperature. The maximum  $P_r$  value of 14  $\mu\text{C}/\text{cm}^2$  was observed for PZT20/80 at the annealing temperature of 500 °C. As the annealing temperature increased from 500 to 600 °C, the PZT30/70 showed the maximum  $P_r$  value of 39  $\mu\text{C}/\text{cm}^2$ . The  $E_c$  increased approximately from 40 to 110 kV/cm as the Ti content increased from 0.47 to 0.8, irrespective of annealing temperature.
3. The dependence of small signal dielectric constant ( $\epsilon_r$ ) of PZT films on Zr/Ti ration and

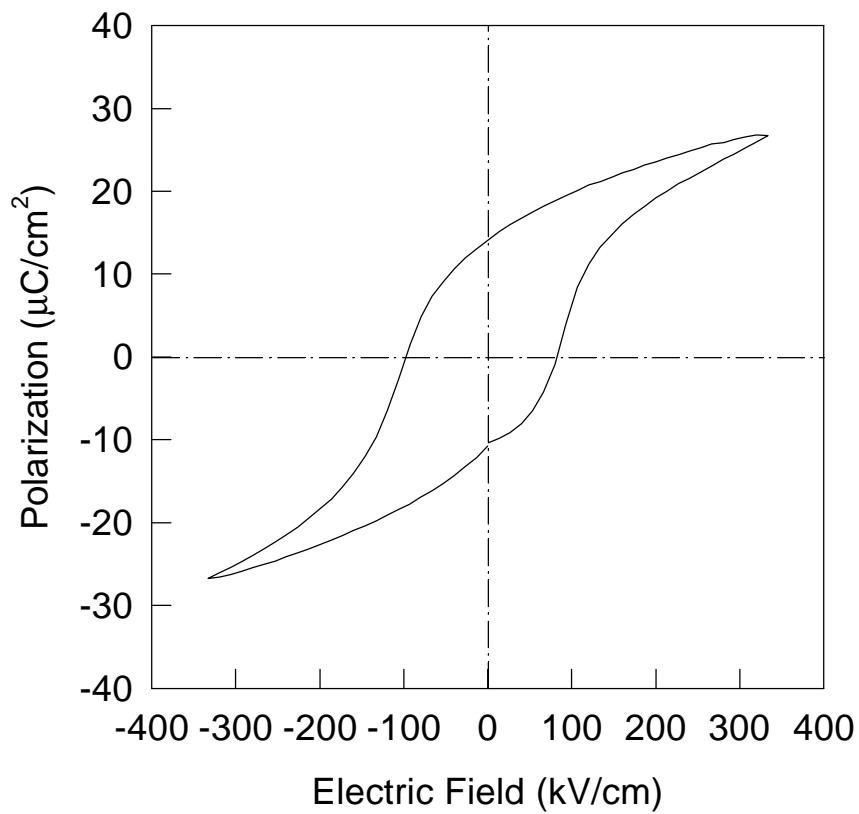
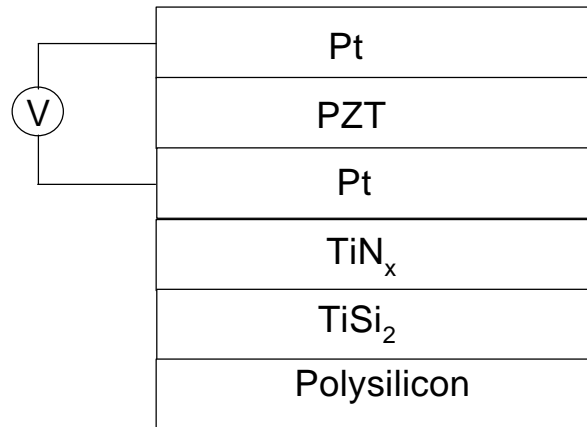


Figure 3.15 a) Hysteresis loop of PZT30/70 films processed on Pt/ $TiN_x$ / $TiSi_2$ /poly-Si at 500 °C by contacting between top Pt and bottom Pt.

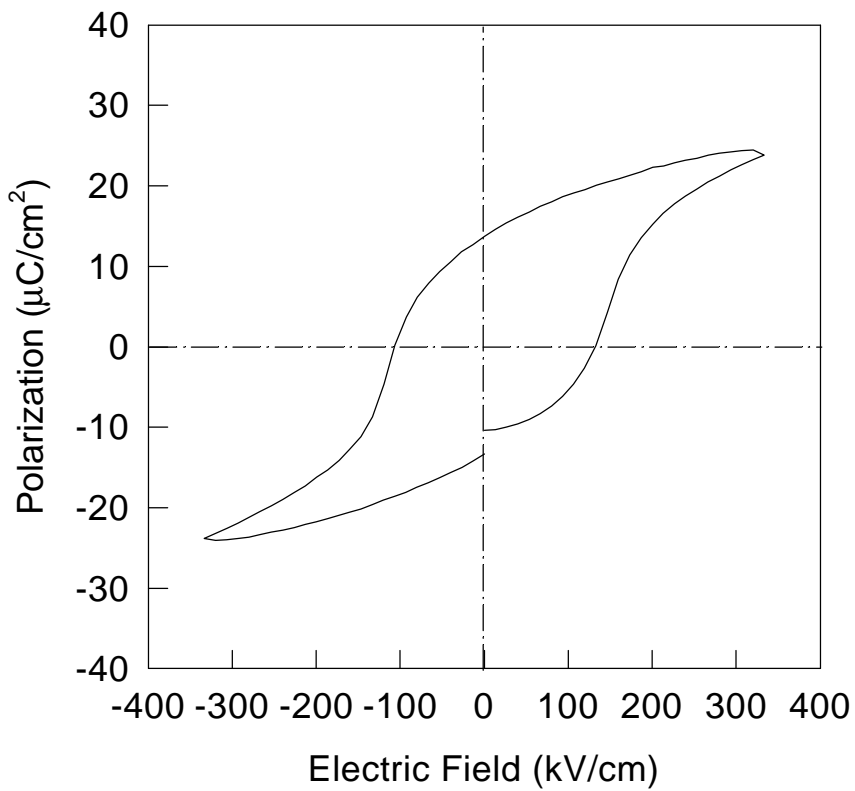
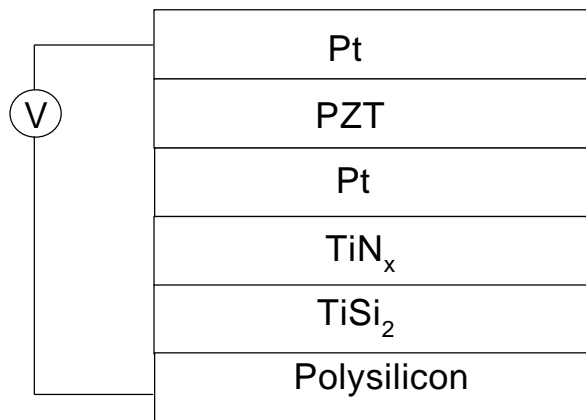


Figure 3.15 b) Hysteresis loop of PZT30/70 films processed on Pt/ $TiN_x$ / $TiSi_2$ /poly-Si at 500 °C by contacting between top Pt and bottom poly-Si.

annealing temperature was investigated. The dependence of  $\epsilon_r$  on the annealing temperature decreased as the Ti content increased. The  $\epsilon_r$  value of PZT20/80 films was not strongly affected by the annealing temperature. The dissipation factor was quite small for the FRAM device applications regardless of the composition and annealing temperature.

4. The fatigue properties of the PZT films were enhanced as the annealing temperature increased. The PZT films annealed at 600 °C showed better fatigue properties than those at 500 °C. It was observed that the polarization degradation was dependent upon the composition. The PZT30/70 and 20/80 films exhibited lesser fatigue problem than the PZT53/47 and 40/60 films.

5. Leakage current density of PZT films processed at 500 °C was investigated as a function of Zr/Ti ratio. It was found that the leakage current density increased at a given applied voltage as the Ti content increased.

6. Currently used diffusion barrier layers (TiN and TiSi<sub>2</sub>) were fabricated on poly-Si by dc sputtering technique, and PZT30/70 films were prepared on Pt/TiN<sub>x</sub>/TiSi<sub>2</sub>/poly-Si substrate for direct integration, and were thermally processed at 500 °C. Well-defined P-E hysteresis loops were observed for the PZT films, indicating that the low temperature processing was compatible with the TiN<sub>x</sub> and TiSi<sub>2</sub> diffusion barrier layers.

### 3.6. REFERENCES

1. B. Jaffe, W. R. Cook, Jr., and H. Jaffe, *Piezoelectric Ceramics*, Academic, New York, (1971).
2. N. Tohge, S. Takahashi, and T. Minami, *J. Am. Ceram. Soc.*, 74, (1991), 67.
3. K. Sreenivas, M. Sayer, and P. Garret, *Thin Solid Films*, 172, (1989), 251.
4. Y. Sakashita, T. Ono, H. Segawa, K. Tominaga, and M. Okada, *J. Appl. Phys.*, 69, (1991),

8352.

5. H. Watanabe, T. Mihara, and C. Paz de Araujo, *ISIF 92 Proceedings*, 139, 1992
6. L. Icker and H. G. Schneider, *Advances in Epitaxy and Endotaxy*, edited by H. G. Schneider, V. Ruth and T. Kormany, Elsevier (1990).
7. S. Goto, N. Fujimura, T. Nishimura, and T. Ito, *J. Crystal. Growth*, 115, (1991), 816.
8. T. Tani, Z. Xu, and D. A. Payne, *Mater. Res. Soc. Symp. Proc.*, 310, (1993), 269.
9. M. Klee, R. Eusemann, R. Waser, W. Brand, and H. van Hal, *J. Appl. Phys.*, 72, (1992), 1566.
10. H. N. Al-Shareef, K. R. Bellur, O. Auciello, X. Chen, and A. I Kingon, *Thin Solid Films*, 252, (1994), 38.
11. H. D. Chen, K. R. Udayakumar, C. J. Gaskey, and L. E. Cross, *Appl. Phys. Lett.*, 67, (1995), 3411.
12. K. Amanuma, T. Mori, T. Hase, T. Sakuma, A. Ochi, and Y. Miyasaka, *Jpn. J. Appl. Phys.*, 32, (1993), 4150.